Pure Appl. Chem., Vol. 76, No. 11, pp. 2027–2049, 2004.

INTERNATIONAL UNION OF PURE AND APPLIED CHEMISTRY

MACROMOLECULAR DIVISION*
WORKING PARTY ON STRUCTURE AND PROPERTIES OF COMMERCIAL POLYMERS**

RHEOLOGICAL PROPERTIES AND ASSOCIATED STRUCTURAL CHARACTERISTICS OF SOME AROMATIC POLYCONDENSATES INCLUDING LIQUID-CRYSTALLINE POLYESTERS AND CELLULOSE DERIVATIVES

(IUPAC Technical Report)

Prepared for publication by
J. L. WHITE[1], L. DONG[1], P. HAN[1], AND H. M. LAUN[2,‡]

[1]*Institute of Polymer Engineering, The University of Akron, Akron, OH 44325, USA;*
[2]*Polymer Physics, BASF Aktiengesellschaft, Ludwigshafen/Rhein, Germany*

*Membership of the Macromolecular Division during the final preparation of this report (2002–2003) was as follows:

***President*:** R. F. T. Stepto (UK); ***Vice President*:** J.-I. Jin (Korea); ***Secretary*:** W. J. Work (USA); ***Titular Members*:** M. Barón (Argentina); M. Hess (Germany); K. Horie (Japan); R. G. Jones (UK); P. Kubisa (Poland); H. M. Laun (Germany); ***Associate Members*:** D. Berek (Slovak Republic); M. Buback (Germany); A. R. Khokhlov (Russia); S. Penczek (Poland); D. Tabak (Brazil); J. Vohlidal (Czech Republic); F. Wang (China); ***National Representatives*:** A. Natansohn (Canada); H. Tenhu (Finland); J.-P. Pascault (France); G. Costa (Italy); R. D. Sanderson (South Africa); J. M. Perena (Spain).

**Contributing Members of the Working Party for this report were as follows:

H. M. Laun (Germany), G. Vassilatos (USA), J. Meissner (Switzerland), M. Fleissner (Germany), H. H. Meyer (Germany), D. J. Groves (UK), L. Utracki (Canada), J. L. White (USA).

‡Corresponding author

Rheological properties and associated structural characteristics of some aromatic polycondensates including liquid-crystalline polyesters and cellulose derivatives

(IUPAC Technical Report)

Abstract: A comparative experimental study of shear-flow rheological properties of thermotropic polymer liquid crystals by eight different laboratories is described. The materials involved four different liquid-crystalline polyesters (LCPs), a glass-fiber-filled liquid-crystalline polyester, hydroxypropyl cellulose (HPC), and two non-liquid-crystalline high-temperature polymers, a poly(etheretherketone) (PEEK), and a polyarylate (PAR). Studies were made in both steady shear-flow and dynamic oscillatory experiments. The data from the various laboratories involved were compared. The level of agreement in the data was much less for most liquid-crystalline polymers than for similar isotropic melts. The Cox–Merz rule is valid for PEEK and PAR, but not for the LCPs and HPC. The occurrence of low levels of extrudate swell and high levels of uniaxial orientation in extrudates of the LCPs and HPC is described.

1. INTRODUCTION

Aromatic polycondensates became increasingly important in the 1980s. Characteristic of these polymers are para-linked aromatic rings in their backbones, which tend to make the chains more rigid than aliphatic hydrocarbon (e.g., vinyl) polymers. While such *p*-linked aromatic polycondensates like poly(carbonate) or poly(ethylene terephthalate) had been known since the 1950s, the full implications were only realized in the 1970s with the discovery that concentrated solutions of poly(*p*-phenylene terephthalamide), poly(*p*-benzamide), and similar polymers exhibited rest state birefringence, liquid-crystalline phases, and associated viscosity reductions [1–3]. These systems are known as lyotropic liquid-crystalline polymers. Similar characteristics were found shortly thereafter with bulk poly(ethylene terephthalate) copolymerized with hydroxybenzoic acid (PHB/PET) [4]. Bulk polymers of this type are said to be thermotropic liquid-crystalline materials. There have been many additional liquid-crystalline polymers (LCPs) synthesized in recent years [5–15]. Many are cited in the patent literature, others in the published scientific literature. In the 1980s, liquid-crystalline polyesters were brought to the marketplace throughout the world beginning with Dartco and Celanese in the USA, and later BASF and ICI in Europe and Idemitsu, Mitsubishi Chemical, Sumitomo Chemical, Unitika, and others in Japan. Other types of liquid-crystalline polymers have also been discovered. Noteworthy has been hydroxypropyl cellulose (HPC), developed originally by Hercules in the early part of the century, but which was not recognized to be a thermotropic polymer liquid crystal until relatively recently [16].

This paper presents a rheological study of the behavior of a series of aromatic polycondensates, including several liquid-crystalline polymers by IUPAC Working Party IV.2.1 on Structure and Properties of Commercial Polymers. The polymers included in this study are poly(etheretherketone) (PEEK), polyarylate (PAR), hydroxypropyl cellulose (HPC), and four different types of liquid-crystalline polyesters plus one type of glass-filled liquid-crystalline polyester.

The high-performance aromatic polycondensate PEEK and the aromatic polyester polyarylate are not liquid crystalline. They are included in the program to allow the different laboratories to compare measurements on aromatic polycondensates at elevated temperatures. The PAR is especially relevant

because it contains an ester linkage like the liquid-crystalline polyesters, which is unstable and subject to hydrolysis. Earlier IUPAC programs involving rheological measurements on polyesters have shown up larger discrepancies than are found with polyolefins [17]. We need to distinguish problems associated with the rheological complexity of polymer liquid crystals and those with chemical instability.

This report describes the contributions of several laboratories and investigators. The names of the laboratories will be abbreviated in the text. These are summarized in Table 1:

Table 1 Contributing laboratories and their representative in the Working Party.

Company/Institution	Location	Abbreviation	Contributor
BASF Aktiengesellschaft	Ludwigshafen, Germany	**BASF**	H. M. Laun
E.I. DuPont de Nemours	Wilmington, Delaware, USA	**DuPont**	G. Vassilatos
Eidgenössische Technische Hochschule Zürich	Zürich, Switzerland	**ETHZ**	J. Meissner
Hoechst	Hoechst, Germany	**Hoechst**	M. Fleissner
Hüls	Recklinghausen, Germany	**Hüls**	H. H. Meyer
ICI	Wilton, UK	**ICI**	D. J. Groves
Industrial Materials Research Institute, National Research Council of Canada	Montreal, Canada	**IMRI**	L. Utracki
Institute of Polymer Engineering, University of Akron	Akron, Ohio, USA	**IPE**	J. L. White

2. EXPERIMENTAL

2.1 Materials

The polymers investigated are detailed with the abbreviations we will use in the text, and their source, in Table 2. The table also gives the measurement temperatures selected for this study. LCP-5 and LCP-5GF are essentially the same in chemical composition except that LCP-5GF is filled with 30 mass % glass fiber.

Table 2 Polymers investigated in this study.

Material	Designation	Supplier	Temperature/°C
Poly(etheretherketone)	**PEEK**	ICI	380
Poly(arylate)	**PAR**	Unitika	300
Liquid-crystalline polyester (unknown composition)	**LCP-1**	Dartco	430
Liquid-crystalline polyester (unknown composition)	**LCP-2**	BASF	300
Poly[*p*-hydroxybenzoate-*co*-(ethylene terephthalate)]. 60/40	**LCP-3**	Tennessee Eastman	250 and 280
Poly[*p*-hydroxybenzoate-*co*-(ethylene terephthalate)]. 60/40	**LCP-4**	Unitika	250 and 280
Poly[*p*-hydroxybenzoate-*co*-(ethylene 1,6-naphthalate)]. 73/27	**LCP-5**	Hoechst Celanese	300
Glass-fiber-filled LCP-5	**LCP-5GF**	Hoechst Celanese	300
Hydroxypropyl cellulose	**HPC**	Hercules, Inc.	180 and 210

The drying conditions for the pellets used by the various laboratories prior to the rheological measurements are summarized in Table 3.

Table 3 Drying conditions (time and temperature in vacuum oven).

	BASF	DuPont	ETHZ	Hoechst	ICI/IMRI	IPE
Temperature/°C	100	120	120	90	90	120 (80 °C for HPC)
Time/hour	24	24	24	24	24	24

The thermal characteristics of the polymers were investigated by IPE using a DuPont 9900 Series differential scanning calorimeter (DSC) and a DuPont thermogravimetric analyzer (TGA). DSC scans at 20 °C per minute for each of the initial and (quenched) samples are shown in Figs. 1a and 1b.

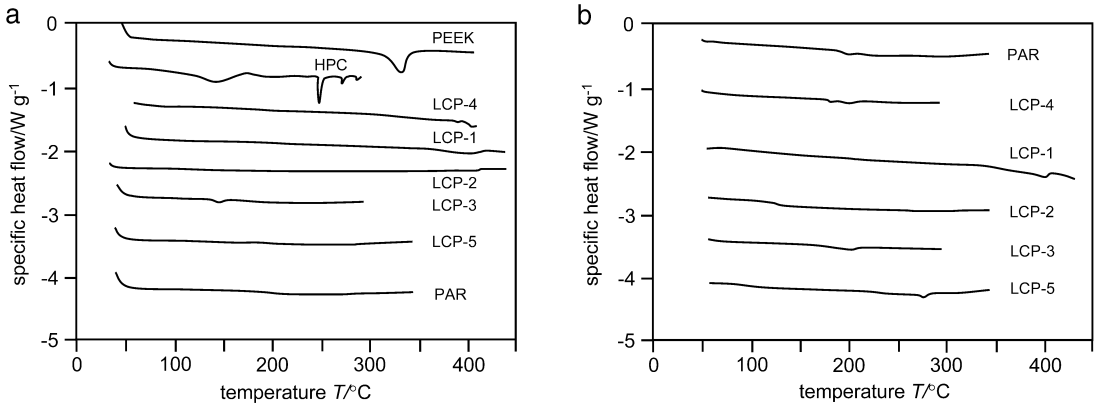

Fig. 1 (a) DSC scans of initial samples; (b) DSC scans of quenched samples.

It may be seen that the initial PEEK sample is crystalline and exhibits a melting point at 340 °C. PAR shows a glass transition temperature around 195 °C. HPC shows a broad shallow transition in the range 120 to 150 °C and other changes in curvature indicating perhaps further transitions. Above 225 °C, degradation seems to set in. LCP-1 shows few features in its DSC trance. Some type of transition is hinted at around 400 °C. LCP-2 (Fig. 1b) shows two minor endothermic peaks around 100 and 285 °C. LCP-3 seems to exhibit a glass-type transition around 70 °C and a very broad transition around 200 °C. It gives evidence of degradation at 375 °C. The first DSC run of LCP-3 exhibits a crystalline melting point at 147 °C and a broad weak melting transition in the vicinity of 200 °C; however, in the second run, the melting transition at low temperature disappeared and that at the high temperature became more significant. LCP-4 has the same chemical composition as LCP-3. LCP-5 shows thermal characteristics in which a series of "slope change" transitions are exhibited below 230 °C. A crystalline melting transition at 280 °C is enhanced after quenching.

Thermogravimetric scans (TGA) at 20 °C increase per minute in air for the various polymers are summarized in Fig. 2a. These suggest an ordering of chemical stability according to the following rating:

PEEK > LCP-1 > LCP-5 > PAR > LCP-2 > LCP-3 > LCP-4 > HPC

TGA isotherms obtained at the respective temperatures of rheological measurements are shown in Fig. 2b. HPC at 210 °C and LCP-1 at 430 °C seem to be the least stable followed by HPC at 180 °C and LCP-2 at 330 °C. The most stable are PEEK (380 °C), PAR (300 °C), and the liquid-crystalline LCP-4 (250 °C), LCP-2 (300 °C), and LCP-3 (250 °C).

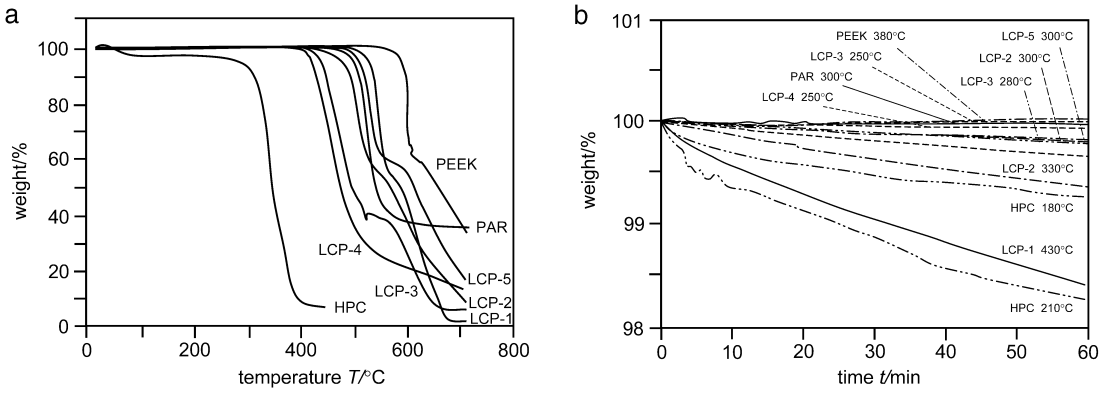

Fig. 2 (a) TGA scan at 20 °C per minute in air; (b) TGA isotherms at test temperatures of Table 2.

Most, if not all, investigators observed that HPC turned brown during the experiments at 180 and 210 °C. ETHZ did not make measurements for this reason. Hoechst and ICI remark that LCP-1 at 430 °C was the most unstable of the polymers under testing conditions studied. It evolves gas and shows significant weight loss.

2.2 Hot-stage polarized microscopy

Several of the polymers were investigated by IPE using a Leitz Laborlux 12 polarized light microscope equipped with a hot stage, which allowed investigations up to 300 °C.

2.3 Melt viscosity from capillary rheometry

Capillary rheometer measurements (mostly using circular dies) have been carried out by several of the laboratories. BASF made measurements with a gas-driven capillary rheometer constructed in their own laboratories. DuPont, ETHZ, and Hoechst all used a piston-driven Goettfert capillary rheometer (Rheograph 2000). IPE applied a piston-driven Instron Capillary Rheometer. ETHZ was the only laboratory that performed measurements with a slit die. The dies used by the different investigators are summarized in Table 4.

Table 4 Dimensions of circular dies used in capillary rheometer experiments.

	BASF	DuPont	Hoechst	IPE
Diameter *D*/mm	0.6, 1.2, 2.0	0.25, 1.0	0.5, 1.0, 2.0, 4.0	1.07–1.57
Length *L*/diameter ratio *L*/*D*	0.25–30	1–10	0.3–30	9.03–43.2

The apparent wall shear rate $\dot{\gamma}_a$ is obtained from the volumetric flow rate Q as

$$\dot{\gamma}_a = \frac{32Q}{\pi D^3}. \tag{1}$$

For a given apparent wall shear rate, the measured extrusion pressure p consists of two contributions: first, the pressure loss in the die, which is four times the wall shear stress σ_w multiplied by the length/diameter ratio L/D of the die. Second, entrance and exit flows contribute to the end correction p_c, also denoted as Bagley correction [18]:

$$p = p_c + 4\ \sigma_w\ L/D \tag{2}$$

Thus, plotting the measured extrusion pressure p for a given apparent wall shear rate versus L/D, the so-called Bagley plot, yields a straight line, the intercept of which with the vertical axis gives p_c, whereas the slope allows a determination of the wall shear stress σ_w.

The true wall shear rate $\dot{\gamma}_w$ was calculated by IPE and DuPont following [19]:

$$\dot{\gamma}_w = \left(\frac{3n+1}{4n}\right)\dot{\gamma}_a \tag{3}$$

Here, n represents the power law exponent derived from the slope of wall shear stress versus apparent wall shear rate in a double-logarithmic plot:

$$n = \frac{d\log\sigma_w}{d\log\dot{\gamma}_a} \tag{4}$$

BASF and Hoechst applied a method described by Laun [20] for the conversion of apparent wall shear rate into true wall shear rate.

The true shear viscosity η finally follows as

$$\eta(\dot{\gamma}_w) = \frac{\sigma_w(\dot{\gamma}_w)}{\dot{\gamma}_w}. \tag{5}$$

ETHZ measured viscosity with a slit die of length L = 50 mm, width W = 10 mm, and slit height H = 0.5 mm. The pressure drop Δp in the barrel was measured using two melt-pressure transducers separated by 50 mm. The wall shear stress follows as

$$\sigma_w = \frac{H\Delta p}{2L}. \tag{6}$$

The apparent wall shear rate is

$$\dot{\gamma}_a = \frac{6Q}{H^2W}. \tag{7}$$

Finally, the true wall shear rate is given by

$$\dot{\gamma}_w = \left(\frac{2n+1}{3n}\right)\dot{\gamma}_a. \tag{8}$$

2.4 Extrudate swell at circular dies

Extrudate swell B, the ratio of extrudate and die diameter, was determined by IPE for LCP-2, LCP-3, LCP-4, LCP-5, and HPC for a capillary of D = 1.07 mm and L/D = 43.2. The data on PEEK and PAR were obtained on a die of D = 1.47 and L/D = 28.9. These length/diameter ratios were chosen to be big enough such that B was independent of die length.

2.5 Structural characterization of extrudates

The extrudates produced in this investigation were characterized by polarized light microscopy, scanning electron microscopy (SEM), and wide-angle X-ray diffraction (WAXS). SEM studies were made by IPE using an ISI-SX-40 scanning electron microscope.

2.6 Steady shear viscosity from cone-plate rheometer

Steady shear-flow viscosities were obtained by IPE on a Rheometrics RMS-800 in a cone-plate mode. From the angular frequency of rotation Ω and the cone angle α, the shear rate $\dot{\gamma}$ is computed as

$$\dot{\gamma} = \frac{\Omega}{\tan \alpha}. \tag{9}$$

The shear stress σ follows from the measured torque M and plate radius R:

$$\sigma = \frac{3M}{2\pi R^3}. \tag{10}$$

2.7 Small-amplitude oscillatory shear measurements

As response to a sinusoidal shear deformation with angular frequency ω and small shear amplitude γ_0, a sinusoidal shear stress of equal angular frequency, but phase-angle δ and amplitude σ_0 is measured. From the decomposition into an in-phase and out-of-phase component, a storage modulus G' and a loss modulus G'' are derived:

$$G' = \frac{\sigma_0}{\gamma_0} \sin \delta \qquad G'' = \frac{\sigma_0}{\gamma_0} \cos \delta. \tag{11}$$

The absolute value of the complex viscosity $|\eta^*|$ follows from the dynamic moduli G' and G'' as

$$|\eta^*(\omega)| = \sqrt{G'^2 + G''^2} \,/\, \omega. \tag{12}$$

For many homogenous non-liquid-crystalline polymers, the empirical Cox–Merz relation [21] was confirmed as a useful approximation:

$$|\eta^*(\omega)| \cong \eta(\dot{\gamma}) \qquad \text{for} \qquad \omega = \dot{\gamma}. \tag{13}$$

This allows determination of the steady-state shear viscosity function $\eta(\dot{\gamma})$ from the measured absolute value of the complex viscosity as a function of angular frequency $|\eta^*(\omega)|$.

ICI, Hoechst, and IMRI made measurements of the dynamic moduli as a function of angular frequency using a Rheometrics mechanical spectrometer. In addition, ICI submitted data as functions of strain amplitude and time for 25-mm-diameter parallel plate geometry. Frequency response between 0.1 and 500 rad/s, at the agreed temperatures, was supplemented by a temperature ramp at fixed angular frequency of 10 rad/s.

The samples were prepared by ICI as follows: Polymer was pressed into a plaque between the rheometer plates to avoid the high pressures and flow in a moulding press. Material was added in several layers using minimum of pressure to obtain an acceptably uniform test specimen of thickness in the range between 1.0 and 1.2 mm. An interval of 10 min was allowed between placing the material between the plates and starting the measurement. This provided a minimum of 5 min soak time at the test temperature. The minimum duration of measurement was about 8 min.

IMRI also used the parallel-plate geometry, whereas Hoechst applied a cone-plate geometry with radius R = 12.5 mm and cone angle $\alpha = 5.7°$ (0.1 rad).

3. RESULTS

3.1 Polarized light microscopy

Polarized light microscopy (PLM) photomicrographs from the different polymers investigated at different temperatures were obtained and studied. PEEK and PAR show no transmission of light. The LCP-2, LCP-3, LCP-4, and LCP-5 exhibit birefringent fields from room temperature to over 300 °C. Above 350 °C, the birefringence intensity decreases. However, from the DSC and TGA studies, the polymers are degrading under these conditions.

3. 2 Capillary rheometry

3.2.1 Bagley plots

Bagley plots of measured extrusion pressure p versus length over radius ratio L/R of the die for various constant apparent wall shear rates $\dot{\gamma}_a$ are shown in Figs. 3a–j. The type of material, the measurement temperature, and the die radius used are given in the diagrams. Figures 3a, c, 3e, 3i, and 3j stem from the BASF nitrogen gas-driven capillary rheometer using a die radius of R = 0.6 mm. Figures 3b, 3d, 3f, 3g, and 3h show data determined by Hoechst using a piston-driven capillary rheometer and a die radius

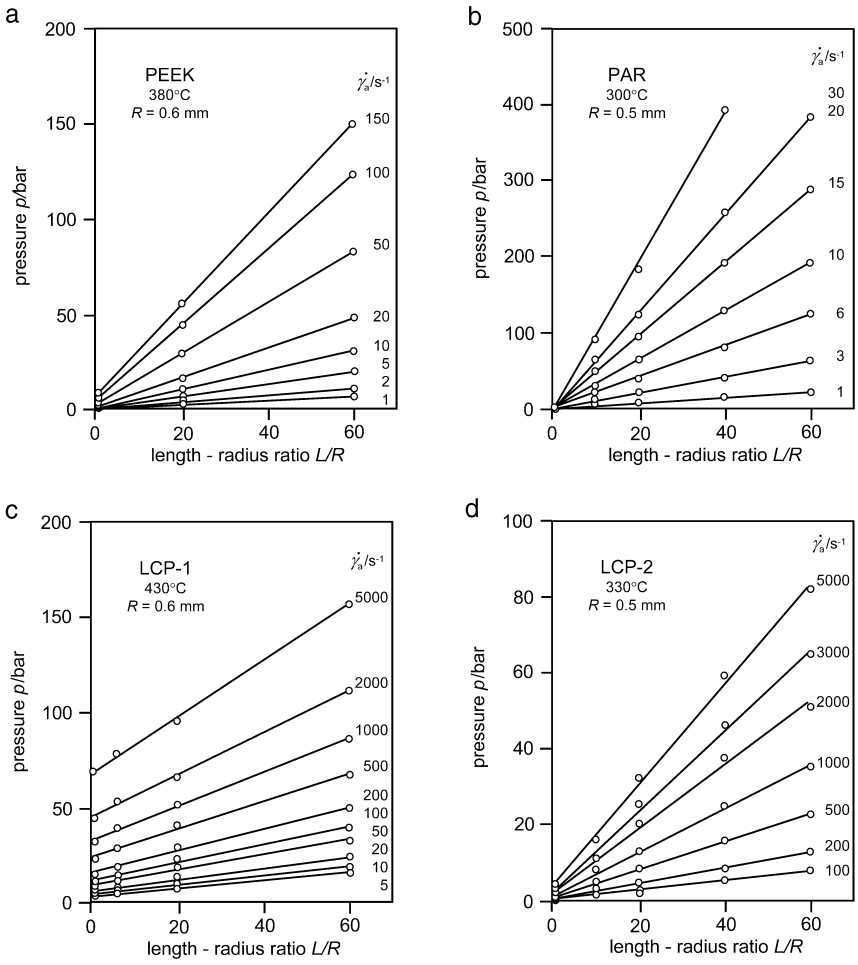

Figs. 3a–j Typical Bagley plots of the materials investigated.

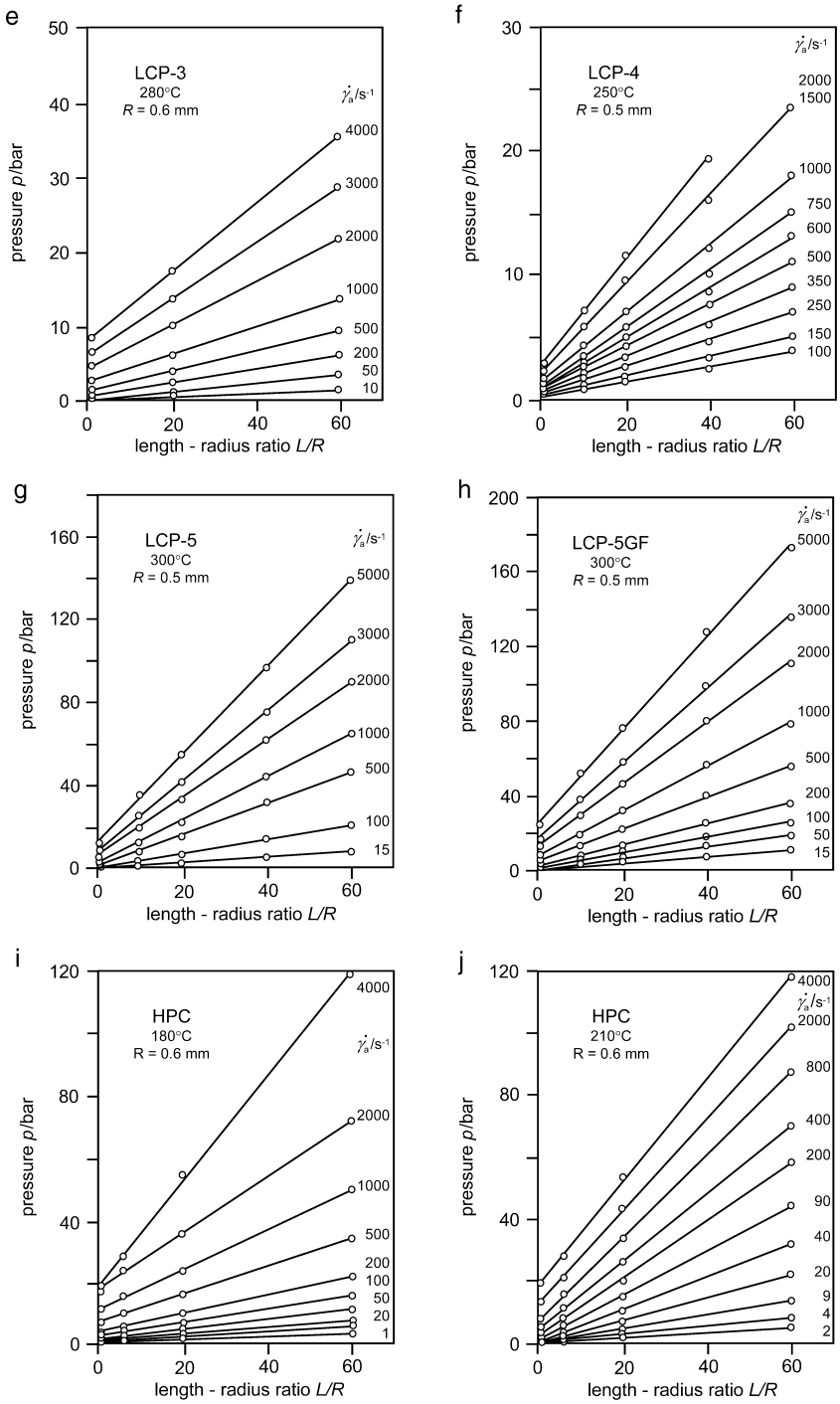

Figs. 3a–j *Continued.*

of R = 0.5 mm. The L/R values cover a rather wide range from orifice (L/R = ≤1) and a long die (L/R = 60). It is noteworthy that the careful measurements yield straight Bagley plots for all materials investigated. Therefore, both the Bagley correction and the wall shear stress can be determined without ambiguity.

3.2.2 Bagley correction versus wall shear stress

The Bagley corrections p_c determined from the various labs are plotted in Figs. 4a–i as functions of the wall shear stress σ_w. The type of material and the measurement temperature, as well as the contributing laboratories, are indicated in the diagrams. For PEEK (Fig. 4a) and PAR (Fig. 4b), the results from BASF and Hoechst agree very well. The Bagley corrections at low shear rates are roughly proportional to the wall shear stress, the ratio p_c/σ_w being in the order of 3 to 5 for PEEK and PAR. For PEEK, the deviation of the results from the other contributing laboratories lies within the range of a factor 0.5 to 2. It is noteworthy that the scatter in general becomes distinctly larger for the liquid-crystalline materials. For HPC (Fig. 4i), the Bagley correction at the higher temperature of 210 °C is distinctly lower than that at 180 °C.

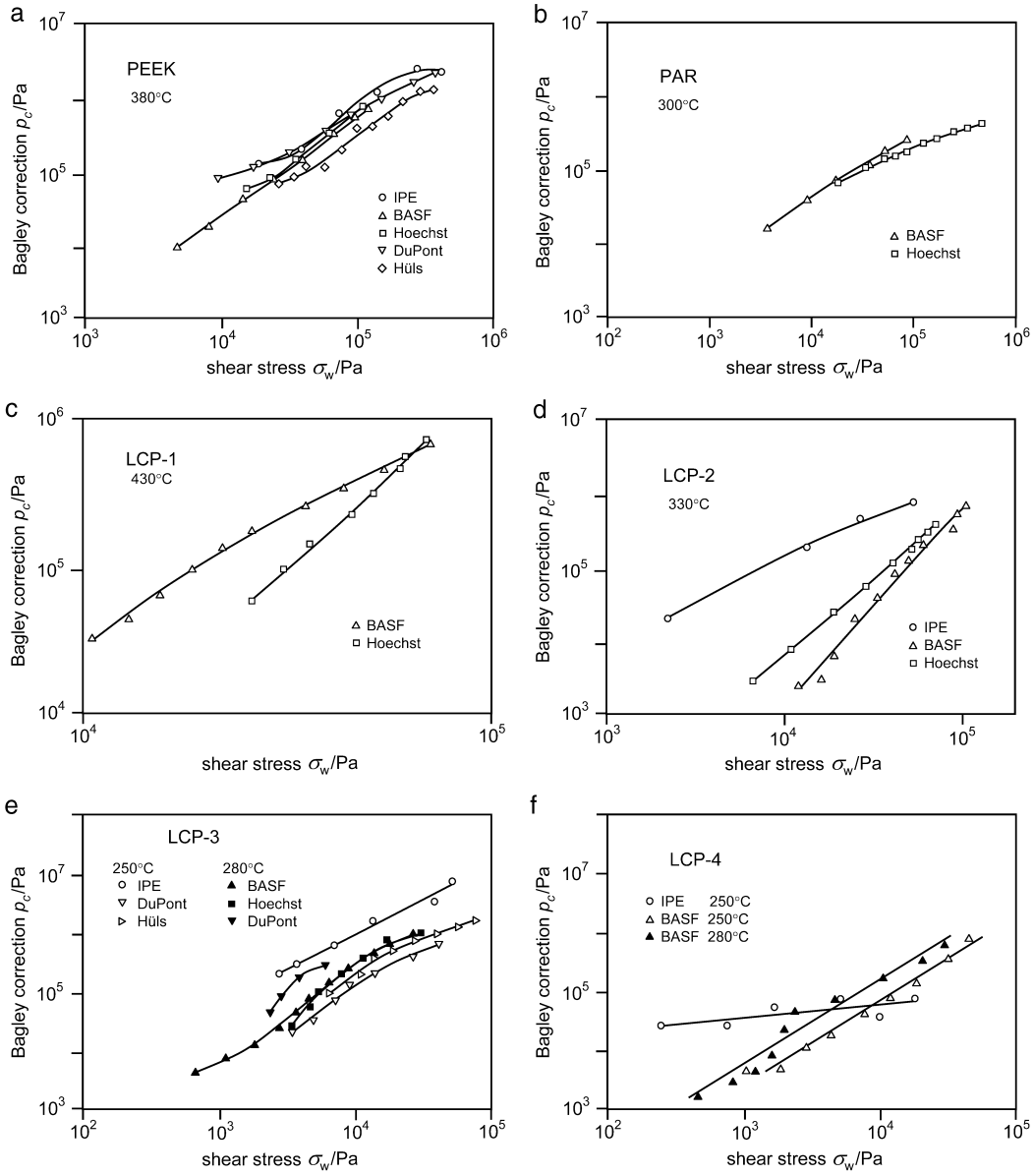

Figs. 4a–i Bagley corrections versus wall shear stress from the various laboratories.

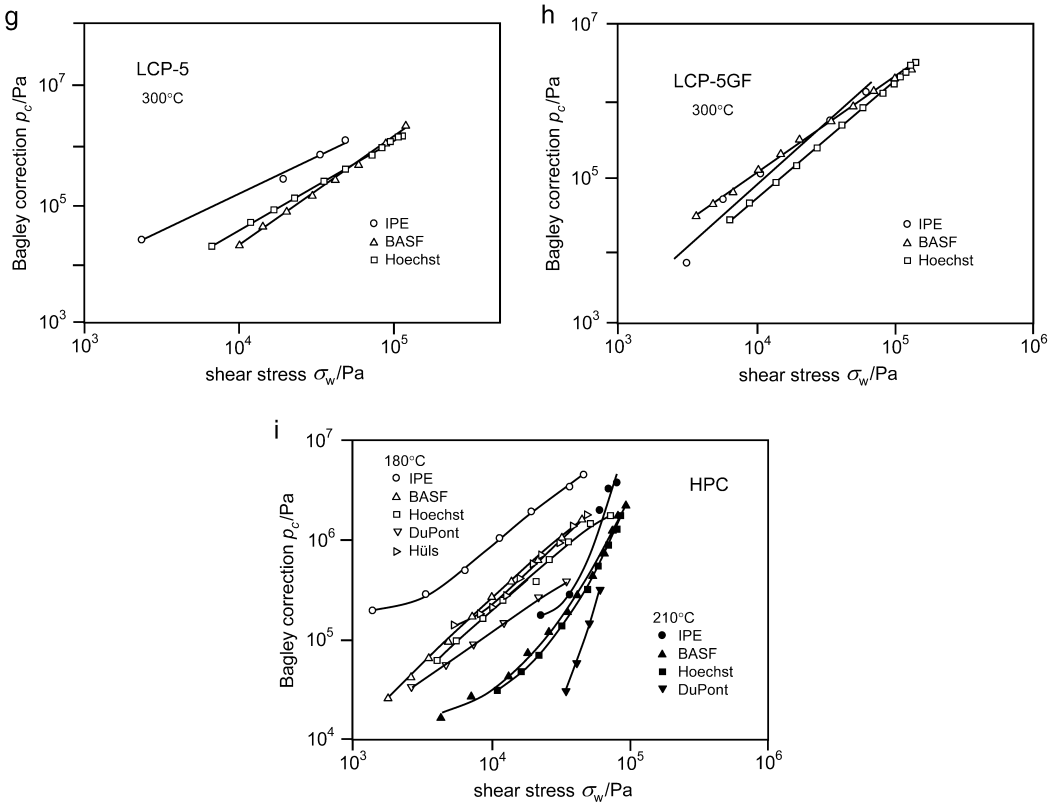

Figs. 4a–i *Continued.*

3.2.3 Shear viscosity function

The true shear viscosity η obtained after applying the Bagley correction as well as a conversion from apparent to true wall shear rate $\dot{\gamma}_w$ is plotted in Figs. 5a–i as viscosity versus wall shear rate, the so-called viscosity function. The type of material and the measurement temperature, as well as the contributing laboratories, are indicated in the diagrams.

PEEK in Fig. 5a exhibits the typical shear-thinning behavior of polymer melts—a decrease of viscosity with increasing shear rate. An excellent agreement between the circular capillary data from IPE, BASF, Hoechst, DuPont, and Hüls is found, whereas the slit die measurements from ETHZ distinctly deviate toward lower viscosity values.

For PAR in Fig. 5b, the capillary data from IPE, BASF, and Hoechst agree well. This material exhibits a quasi-Newtonian regime with constant viscosity up to a shear rate $\dot{\gamma}_w = 100\ s^{-1}$. The viscosity level is confirmed by cone-plate results from IPE, using the Cox–Merz rule, which extend to a shear rate as low as $0.01\ s^{-1}$.

LCP-1 was investigated by BASF, Hoechst, and Hüls at 430 °C. Hoechst reported the development of volatiles under the conditions of the experiment. The shear viscosity data measured by Hüls (Fig. 5c) show a viscosity decrease with increasing shear rate exhibiting a power law behavior: $\eta \propto \dot{\gamma}_w^n$.

LCP-2 (Fig. 5d) was characterized at 300 and 330 °C by BASF, by Hoechst at 330 °C, and by IPE at 300 °C. The shear viscosity decreases with increasing shear rate. BASF and Hoechst data obtained at 330 °C differ from their mean by 20 %. IPE found the viscosity at that temperature too low for a reliable measurement. At 300 °C, the IPE and BASF data closely agree.

LCP-3 (Fig. 5e) was measured both at 250 and 280 °C by BASF, DuPont, Hoechst, Hüls, and IPE. Cone-plate data at 250 °C from IPE are added to the diagram. Generally, the viscosity decreases

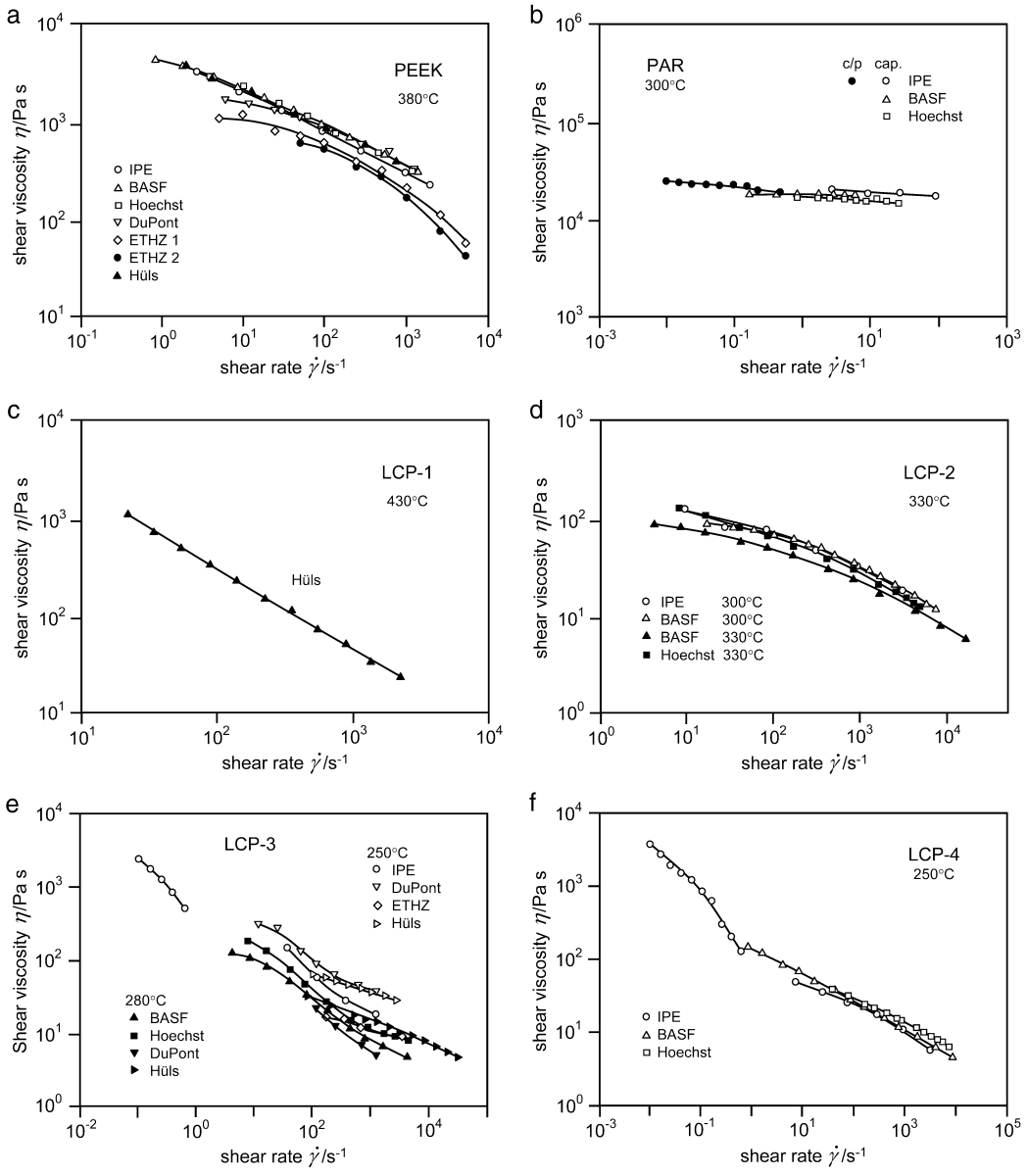

Figs. 5a–i Bagley corrected true shear viscosity versus true wall shear rate from the various laboratories.

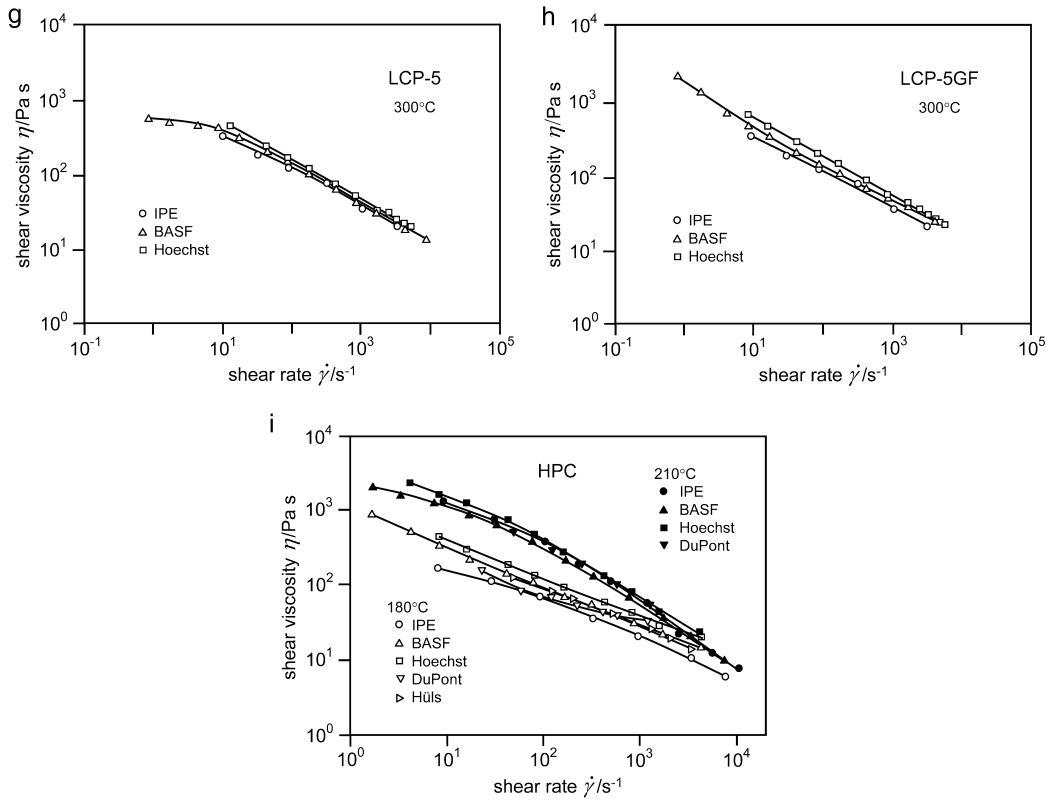

Figs. 5a–i *Continued.*

strongly with increasing shear rate. There is very significant scatter in the data from different laboratories. At 280 °C, the Hoechst and Hüls data are higher than those of BASF and DuPont. The data spread at 100 s^{-1} is ±30 %, from the mean. At 250 °C, the DuPont, Hüls, and IPE data are higher than the ETHZ data. The scatter at 100 s^{-1} is ±50 % from the mean. The low-shear-rate cone-plate rheometer data are roughly consistent with the capillary rheometer data.

LCP-4 (Fig. 5f) was characterized at 250 °C by BASF, Hoechst, and IPE. The viscosity decreases with increasing shear rate. The agreement between the capillary data from the various laboratories is good. IPE cone-plate measurements are added, which seem consistent with the capillary rheometer results in the overlapping shear rate regime. However, the increase of viscosity with decreasing shear rate is much stronger—approximately inversely proportional to the shear rate—indicating an apparent yield stress of the order of $\sigma_y \approx 100$ Pa (i.e., the melt will not flow at shear stresses below σ_y).

LCP-5 (Fig. 5g) and LCP-5GF (Fig. 5h) were characterized at 300 °C by BASF, Hoechst, and IPE. The viscosity of the pure material at 100 s^{-1} is about 120 Pa·s. The scatter remains within ±5 % of the mean shear viscosity of the reporting laboratories. The viscosity for the glass-fiber-reinforced material LCP-5GF is about 140 Pa·s at 100 s^{-1}, and the data from the laboratories are within ±30 %.

HPC (Fig. 5i) clearly exhibits a lower shear viscosity at the higher temperature of 210 °C: At 100 s^{-1}, the HPC at 180 °C has a mean viscosity of about 110 Pa·s with a spread of ±40 %. At 210 °C, the viscosity is about 400 Pa·s, the data spread being ±5 %. The 210 °C data tend to become Newtonian at lower shear rates. At 180 °C, however, the material seems to retain its non-Newtonian character at the lowest shear rates investigated, the upward curvature even slightly increasing.

3.3 Extrudate swell

The extrudate swell B of the various polymers investigated was determined by IPE and is shown in Fig. 6. The results may be divided into two groups: PEEK, PAR, and HPC at 210 °C have values of $B > 1.1$. HPC at 180 °C, LCP-2, LCP-3, LCP-4, and LCP-5 all have values of $B < 1.1$.

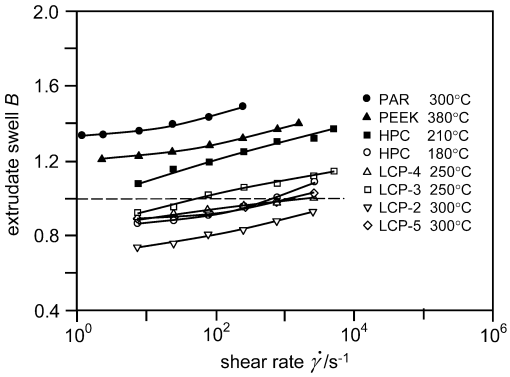

Fig. 6 Extrudate swell as a function of wall shear rate for the various polymers investigated. Die dimensions for LCPs and HPC: D = 1.07 mm, L/D = 43.2; for PAR and PEEK: D = 1.57 mm, L/D = 29.

3.4 Structural studies of extrudates

SEM photomicrographs of extrudates fractured in liquid were investigated. The PEEK and PAR extrudates showed coherent solid brittle fracture surface. The various liquid-crystalline polyester extrudates also exhibit fibrillar characteristics. It is easier to "peal" the extrudates of LCP-2 than LCP-5. The HPC fibers also showed fibrillar fracture surface.

WAXS film patterns for the extrudates were obtained and examined. PEEK shows no orientation in its WAXS patterns. PAR exhibits no obvious structure. The HPC at 180 °C and the various liquid-crystalline polyester extrudates and HPC at 180 °C exhibit significant uniaxial orientation as represented by the equatorial concentrations of reflections.

3.5 Oscillatory shear measurements

Dynamic measurements were made primarily by ICI. There were also contributions from Hoechst and IMRI. We will first present amplitude sweeps at constant angular frequency in order to show the limits of linear viscoelastic behavior, indicated by a decrease of the dynamic moduli with increasing amplitude. This test is required to select the appropriate shear amplitude γ_0 for the measurements. Second, the stability of the melts is investigated by means of time sweeps at a given angular frequency ω. They indicate the acceptable time window for the measurements. Thirdly, the frequency dependence of the dynamic moduli and of the absolute value of the complex viscosity are presented based on frequency sweeps using the parameters of the pre-measurements presented before. Where appropriate, temperature sweeps at given angular frequency are also presented.

3.5.1 Amplitude sweeps

The measurements are shown in Figs. 7a–f. The measurement temperature and the angular frequency are indicated in the graph. No amplitude dependence up to $\gamma_0 = 0.2$ is found for PEEK (Fig. 7a). The same is true for PAR, although not shown by a diagram. Due to the high measurement temperature of 430 °C for LCP-1, most measurements were made using prepressed discs. The moduli are extremely strain sensitive (Fig. 7b), so $\gamma_0 = 0.05$ was used for the additional measurements. A distinct, but less severe amplitude dependence is also found for LCP-2 (Fig. 7c). Data for LCP-3 (Fig. 7d) are shown for

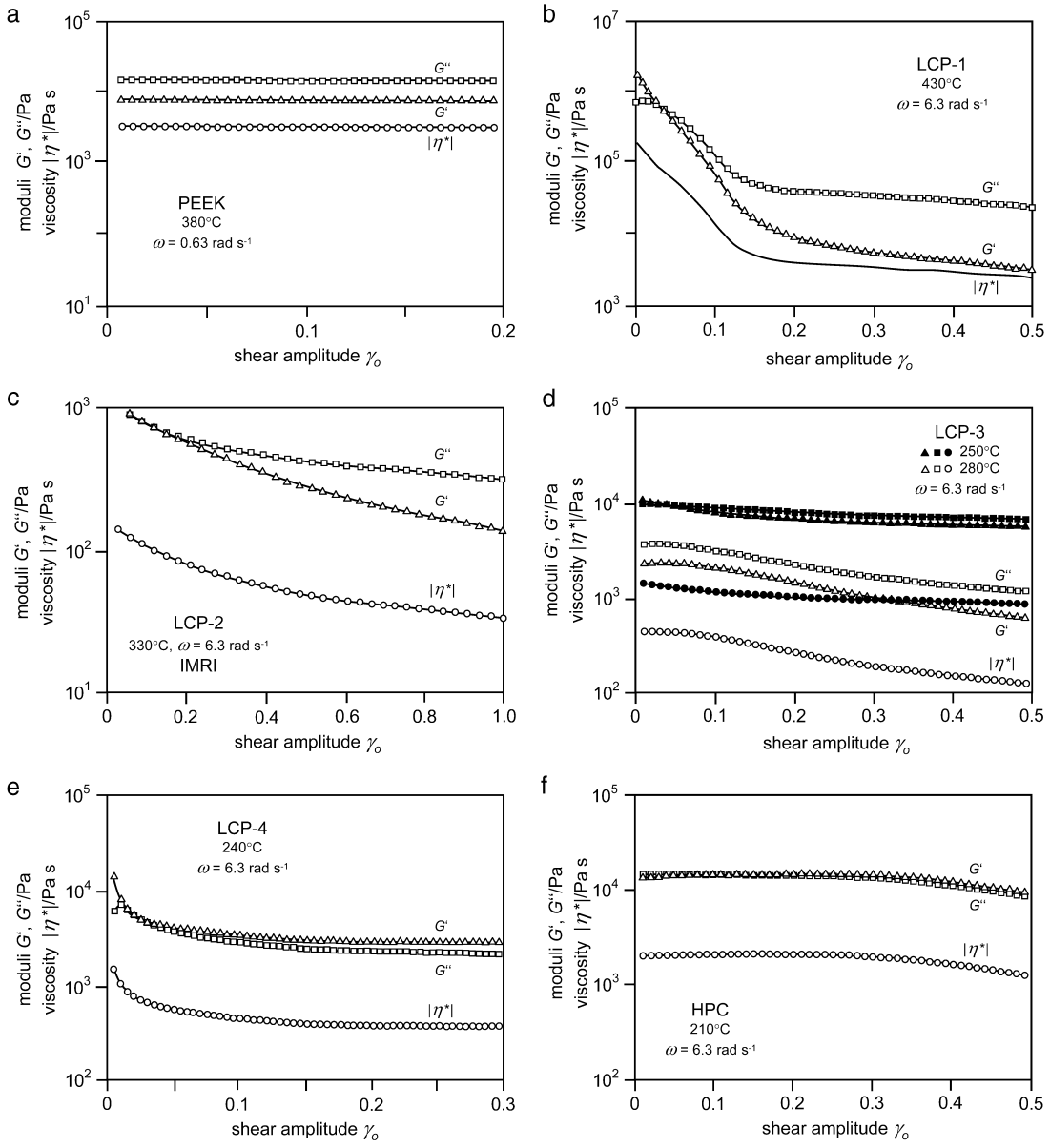

Figs. 7a–f Examples for amplitude sweeps on the various samples.

both 250 °C (full symbols) and 280 °C (open symbols). Here, the amplitude dependence is very weak at the lower temperature. LCP-4 in Fig. 7e exhibits a strong increase of the moduli when the amplitude approaches 0.01. Interestingly, for HPC the moduli remain constant up to $\gamma_0 \approx 0.3$.

3.5.2 Time sweeps

Stability measurements are shown in Figs. 8a–e. PEEK exhibits a slow increase of the moduli with time (Fig. 8a), about 30 % of *G*' for 30 min. PAR remains stable (not shown by a diagram). LCP-1 in Fig. 8b shows a distinct increase with time. LCP-3 (Fig. 8c) at 280 °C remains fairly stable, whereas LCP-4 (Fig. 8d) at 240 °C shows a weak increase with time, which is more pronounced for the storage moduli. Increasing moduli with time are also found for HPC in Fig. 8e.

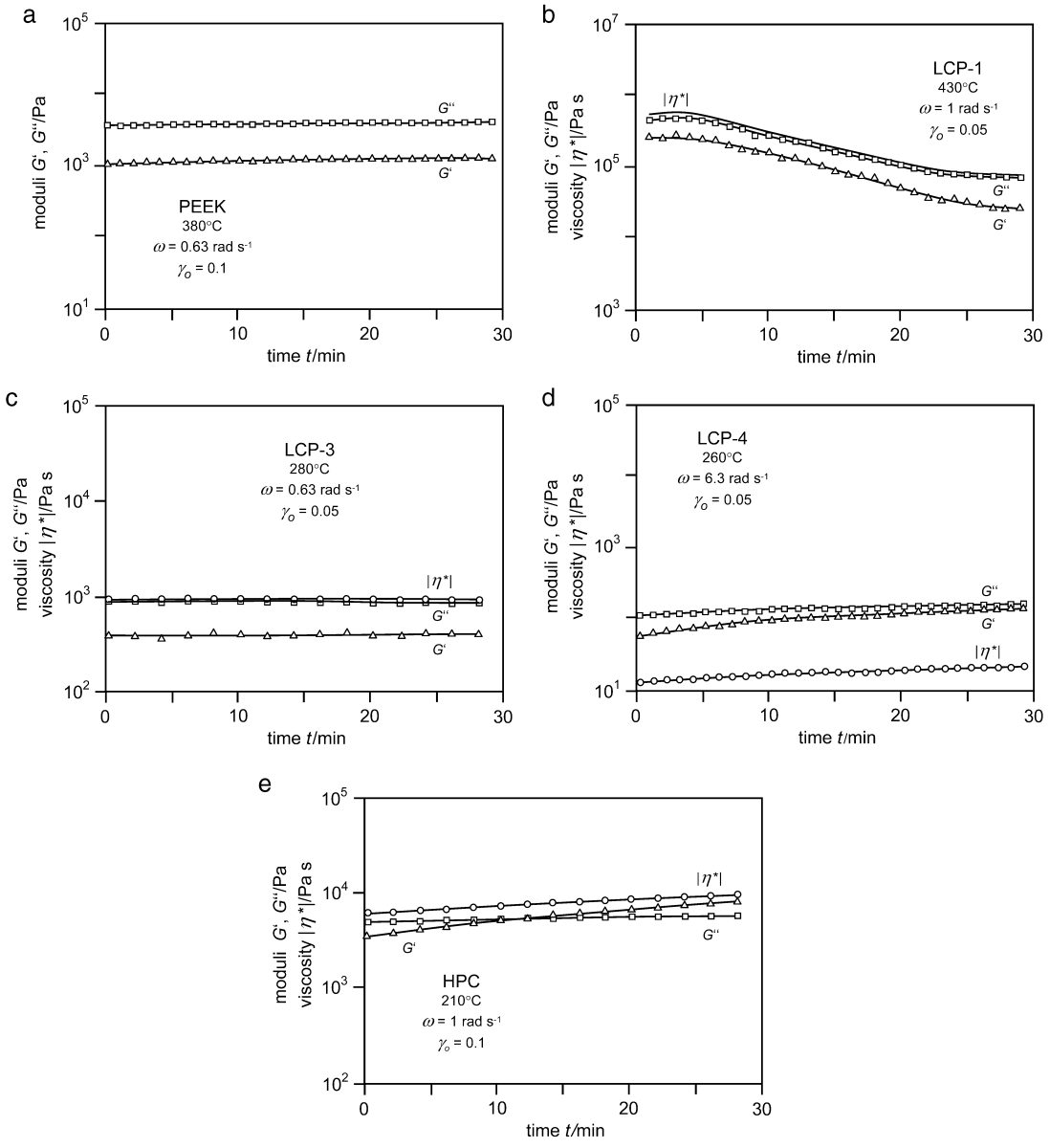

Figs. 8a–e Examples for stability measurements on the various samples.

3.5.3 Frequency sweeps

The results are summarized in Figs. 9a–i. PEEK (Fig. 9a) exhibits the normal behavior of a homogeneous melt: Both moduli decrease with decreasing angular frequency toward the terminal zone, while the slope of G' is bigger than that of G''. As a consequence, the viscosity tends to reach a plateau, the zero shear rate viscosity, with decreasing angular frequency. The results from ICI and Hoechst agree rather well. A similar behavior is found for PAR in Fig. 9b. Here, the viscosity plateau at low angular frequencies is more evident.

The behavior of LCP-1 (Fig. 9c) is similar to that of the homogeneous melts above. In contrast, LCP-2 (Fig. 9d) shows a behavior which is characterized by nearly a constant ratio of G'/G'' over a wide range of angular frequencies (0.1–628 rad/s). The dependence of the moduli on angular frequency may

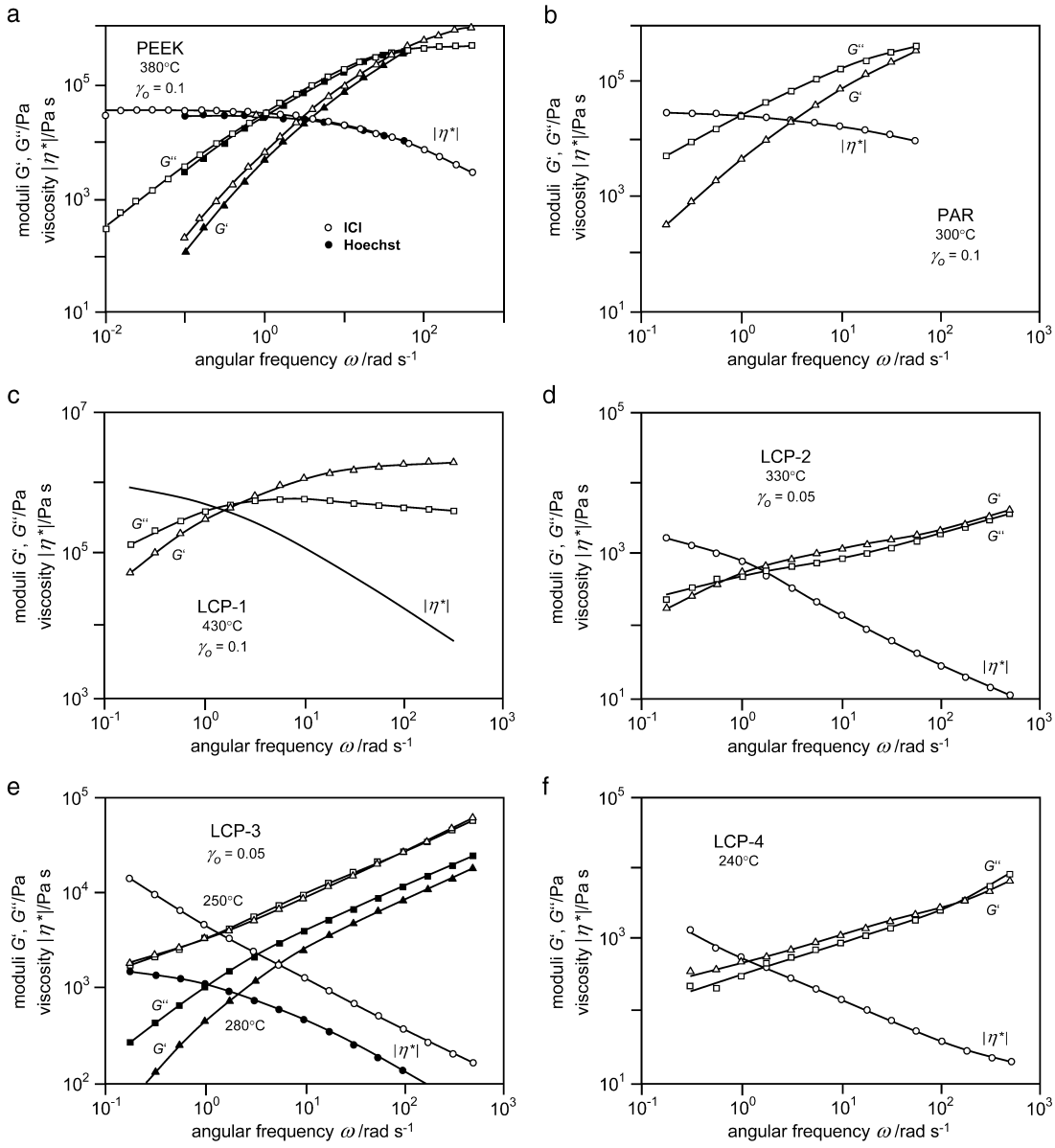

Figs. 9a–i Frequency dependence of the dynamic moduli and of the resulting absolute value of the complex viscosity of the various samples.

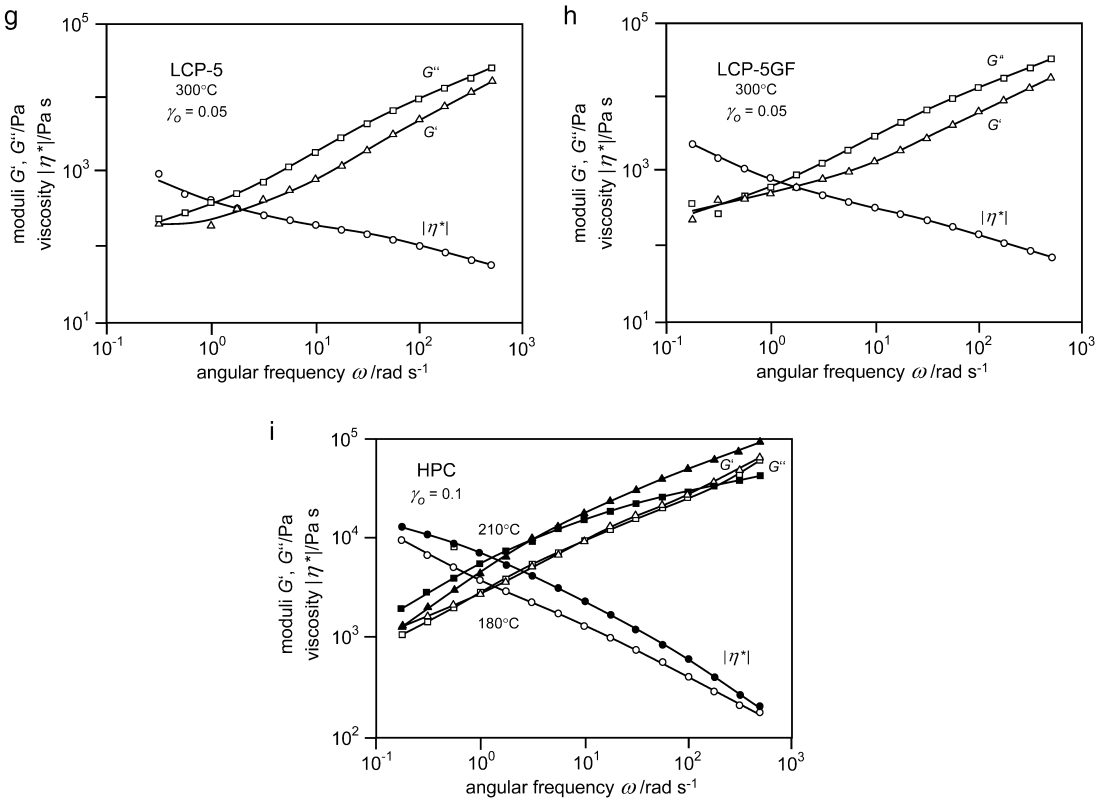

Figs. 9a–i *Continued.*

be approximated by a power law $G' \approx G'' \propto \omega^s$, with an exponent $s \approx 0.45$. Such behavior is typical for melts with some internal structure. As a consequence, the shear-thinning behavior of the viscosity is weak. Below 1 rad/s, however, the transition toward the terminal zone becomes visible.

A nearly constant ratio of both moduli over the whole range of frequencies investigated is also found for LCP-3 (Fig. 9e) at 250 °C. In addition, the moduli decrease with decreasing frequency becomes less steep at the lowest frequencies. As a consequence, the viscosity shows a clear upswing with decreasing angular frequency. The low-frequency behavior at 280 °C is opposite: Both moduli show a more pronounced decrease with decreasing angular frequency (onset of the terminal regime), which causes the viscosity to level off toward a zero shear rate viscosity.

LCP-4 (Fig. 9f) exhibits a weakly increasing ratio of G' and G'' with decreasing angular frequency, which again causes an upswing of the viscosity with decreasing angular frequency. Principally, a similar trend is found for both LCP-5 (Fig. 9g) and LCP-5GF (Fig. 9h). The addition of glass fibers causes the viscosity level compared to the neat polymer to increase.

HPC in Fig. 9i shows a nearly constant ratio of the moduli at 180 °C (open symbols) over nearly the whole range of angular frequencies investigated. The slope is approximated by $G' \approx G'' \propto \omega^{0.5}$, which causes a viscosity proportional to $\omega^{-0.5}$. Interestingly, at 210 °C the material exhibits a higher viscosity than at 180 °C. In addition, the shape of the moduli and of the viscosity versus angular frequency corresponds to that of a normal melt: G' decreases more strongly than G'' with decreasing angular frequency and the viscosity tends toward a plateau value.

3.5.4 Temperature sweeps

IMRI ran temperature sweeps on the samples. Two are shown in Figs. 10a–b. For LCP-2 (Fig. 10a), only a weak decrease of the moduli is observed in the range 275–325 °C. Above, a strong decrease indicates the onset of thermal degradation. Below 275 °C, the melt viscosity increases steeply.

When LCP-3 (Fig. 10b) is heated up from 180 °C, the moduli and the viscosity first increase with increasing temperature up to about 220 °C. Above, the results show a steep decrease, and finally reach a quasi-plateau at about 260 °C. A subsequent decrease of the temperature starting from 280 °C causes the moduli and viscosity to remain on the low plateau even below 260 °C. The values then increase more strongly with decreasing temperature and finally reach the starting levels of 180 °C.

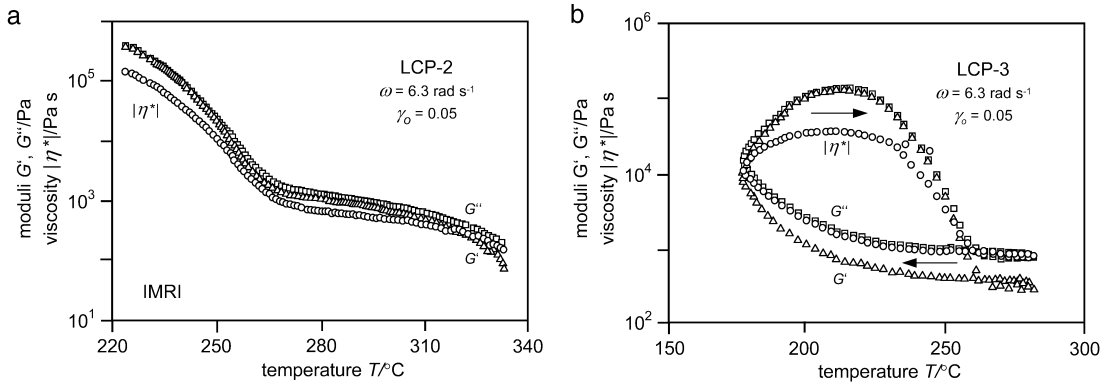

Fig. 10 Temperature sweeps by IMRI on LCP-2 (a) and LCP-3 (b).

4. DISCUSSION

4.1 Rheological data summary of mean behavior

4.1.1 PEEK and PAR

Certain clear trends exist. PEEK and PAR are isotropic melts of flexible polymers, which generally exhibit $\eta(\dot{\gamma})$ decreasing with shear rate, $|\eta^*(\omega)|$ decreasing with frequency and $G''(\omega) > G'(\omega)$ in the terminal zone. Cone-plate and capillary data agree. The Cox–Merz relation (eq. 13) is found to be valid for both PEEK and PAR. The value of Δp_{ends} for PAR is 3 to 4.5 times σ_w, a reasonable value for relatively narrow molecular weight distribution polymer melts. Data from different laboratories are in close agreement.

4.1.2 HPC

Polarized light microscopy shows that HPC is liquid crystalline at 180 °C and predominantly isotropic at 210 °C. As a consequence, the 180 °C viscosity is lower than that at 210 °C, a striking observation confirmed by earlier investigators [22,23].

The 210 °C shear viscosity data from the different laboratories are in close agreement. However, different for truly isotropic melts, one finds $|\eta^*(\omega)| \approx 4\eta(\dot{\gamma})$.

The 180 °C data exhibit considerable scatter. The end pressure losses are much greater than at 210 °C and also greater than for PEEK and PAR when evaluated at the same shear stress. From the dynamic data HPC at 180 °C, the liquid-crystalline behavior is indicated by a constant ratio of storage and loss modulus over a wide range of angular frequencies. Furthermore, $|\eta^*(\omega)| \approx 8\eta(\dot{\gamma})$ indicates the Cox–Merz relation is not valid.

4.1.3 LCP-1

The LCP-1 polymer at 430 °C seems highly unstable compared to the other polymers in this investigation. The frequency response of the moduli, however, is similar to that of an isotropic melt in the investigated range.

4.1.4 LCP-2

The LCP-2 at 330 °C seems to have a tendency to reach a viscosity plateau at low shear rates or angular frequencies, respectively. At higher angular frequencies, however, a nearly constant ratio of the storage and loss modulus is found. $|\eta^*(\omega)| \approx 8\eta(\dot{\gamma})$ indicates the Cox–Merz relation is not valid. The ends pressure loss data from the different laboratories are not consistent.

4.1.5 LCP-3/LCP-4

LCP-3 at 250 °C does not show a tendency to reach a low shear rate Newtonian viscosity, and the ratio of G'/G'' remains constant over a wide range of angular frequencies. Δp_{ends} is rather large compared to σ_w. The Cox–Merz relation is not valid.

The dynamic data of LCP-3 at 280 °C are similar to those of an isotropic melt, at least in the low angular frequency regime. Cone-plate shear viscosity data are somewhat higher, but more or less consistent with capillary results. The behavior is qualitatively similar to earlier rheological studies of this material in the literature [21,24].

LCP-4 at 240 °C behaves rather similarly to LCP-3 at 250 °C. It is believed by many researchers that LCP-3 (and perhaps also LCP-4) are two-phase materials with one phase being almost pure PET [21,23]. This phase may be partially crystalline at 250 °C, but has melted at 280 °C.

4.1.6 LCP-5/-5GF

The trends are similar to the other LCPs. The addition of glass fibers causes the viscosity level to increase. $|\eta^*(\omega)|$ is significantly greater than $\eta(\dot{\gamma})$.

4.2 Extrudate swell and structure

Extrudate swell of the LCPs and HPC is much lower than that for PEEK and PAR. The PEEK and PAR data are typical of extrudate swell of isotropic condensation polymers. The ranking of extrudate swell B may be expressed by:

PAR > PEEK > HPC (at 210 °C) > 1

LCP-3 (at 250 °C) ≈ 1

1 > LCP-4 ≈ LCP-5 ≈ HPC (at 180 °C) > LCP-2

The extrudates of the liquid-crystalline polymers including LCP-2, LCP-3, LCP-4, LCP-5, and HPC at 180 °C seem from SEM to be fibrillar in character, and from WAXS to contain significant crystalline orientation. This is very much in agreement with earlier studies of Shimamura et al. [16] on HPC and Sugiyama et al. [25] on LCP-4 among others. The LCP-5 has noticeably lower WAXS orientation than LCP-2, LCP-3, LCP-4, or HPC at 180 °C. It would seem that rheological data, SEM results on extrudates, and WAXS data on extrudates suggest LCP-5 is, in some sense, less liquid crystalline than the other samples.

4.3 Level of agreement of rheological data among different laboratories

In Table 5, we summarize viscosity measurements of the polymer melts of this study and the magnitude of data scatter from different laboratories. Agreement was obtained (with the exception of one laboratory) for PEEK, PAR, and non-liquid-crystalline HPC (210 °C) of ±50 %. The smallest scatter levels are found with the LCP-5 and the greatest with the HPC (180 °C) and LCP-3.

Table 5 Comparison of shear viscosity data for different laboratories.

Sample	*T*/°C	No. of labs making measurements	Shear viscosity η at 100 s^{-1}/Pa·s	Magnitude of scatter from mean
PEEK	380	5	800	±15 % (5 labs)
				±5 % (4 labs)
PAR	300	3	20 000	±5 %
LCP-1	430	3		
LCP-2	300	2	80	±15 %
	330	2	60	±20 %
LCP-3	250	4	50	±50 %
	280	4	30	±30 %
LCP-4	250	3	130	±10 %
LCP-5	300	3	130	±5 %
LCP-5GF	300	3	160	±10 %
HPC	180	5	110	±40 %
	210	4	400	±5 %

The good agreement in the PEEK and PAR data and the HPC (210 °C), but the scatter of the HPC (180 °C) suggests that liquid crystallinity is the major source of disagreement of scatter in rheological data from different laboratories. The reasons for the differences among the five liquid-crystalline polyesters are not as clear. The best reproducibility was found for LCP-5, the least for LCP-3. The former material would seem to have the lowest level of liquid crystallinity, the latter to contain amounts of an unmelted phase.

5. SUMMARY AND CONCLUSIONS

A joint experimental study was conducted, comparing the rheological characteristics of various liquid-crystalline polyesters and other thermoplastic polycondensates. Two aromatic polycondensates without liquid-crystalline character, PEEK and PAR exhibit zero shear viscosities, obey the Cox–Merz relation, and show die end pressure losses and extrudate swell typical of normal linear thermoplastics. Liquid-crystalline polyesters and liquid-crystalline HPC show typical differences in the dynamic moduli versus angular frequency. Distinct deviations from the Cox–Merz rule are found, the absolute value of the complex viscosity being much higher than the steady shear viscosity from capillary rheometry. They exhibit larger ends pressure losses and much less extrudate swell. The agreement of data between the different laboratories is generally better for the isotropic PEEK and PAR, and much poorer for the liquid-crystalline polymers.

6. LIST OF SYMBOLS

B	extrudate swell
D	capillary diameter
G'	storage modulus
G''	loss modulus
H	slit die height
L	capillary length
M	torque
n	power law coefficient
p	extrusion pressure
p_c	entrance pressure loss (Bagley correction)
Q	volumetric flow rate
R	plate radius
W	slit die width
α	cone angle
δ	phase angle
Δp	pressure drop
$\dot{\gamma}$	shear rate
$\dot{\gamma}_a$	apparent wall shear rate
$\dot{\gamma}_w$	true wall shear rate
γ_0	shear amplitude
η	shear viscosity
$\lvert\eta^*\rvert$	absolute value of the complex viscosity
σ	shear stress
σ_w	wall shear stress
σ_0	shear stress amplitude
σ_y	yield stress
ω	angular frequency
Ω	angular frequency of shaft rotation

ACKNOWLEDGMENTS

The authors would like to thank Prof. Judith E. Puskas (University of Western Ontario, UWO, Canada), Yongmoon Kwon (UWO), and Gerhard Schmidt (BASF) for substantial help in editing the figures.

REFERENCES

1. S. L. Kwolek. U.S. Patent 3,671,542 (1972).
2. S. P. Papkov, V. G. Kulichikhin, V. P. Kalmykova, A. Ya. Malkin. *J. Polym. Sci. Polym. Phys.* **12**, 1753 (1974).
3. H. Aoki, J. L. White, J. F. Fellers. *J. Appl. Polym. Sci*. **23**, 2293 (1979).
4. W. J. Jackson and H. F. Kuhfuss. *J. Polym. Sci. Polym. Chem. Ed.* **14**, 2043 (1976).
5. S. G. Cottis, J. Economy, B. E. Nowak. U.S. Patent 3,637,595 (1972).
6. T. C. Pletcher. U.S. Patent 3,991,014 (1976).
7. G. W. Calundann. U.S. Patent 4,067,852 (1978).
8. R. J. Schaefgen. U.S. Patent 4,075,262 (1978).
9. A. J. East and G. W. Calundann. U.S. Patent 4,318,841 (1982).
10. J. I. Jin, S. Antoun, C. Ober, R. W. Lenz. *Br. Polym. J.* **12**, 132 (1980).
11. B. P. Griffin and M. K. Cox. *Br. Polym. J.* **12**, 147 (1980).

12. R. W. Lenz and J. I. Jin. *Macromolecules* **14**, 1405 (1981).
13. O. D. Decz. U.S. Patent 4,390,681 (1983).
14. B. Hisgen, H. J. Kock, M. Portugall, E. Seiler, G. Blinne. U.S. Patent 4,748,229 (1988).
15. H. J. Kock. U.S. Patent 4,778, 927 (1988).
16. K. Shimamura, J. L. White, J. F. Fellers. *J. Appl. Polym. Sci*. **26**, 2165 (1981).
17. J. L. White and H. Yamane. *Pure Appl. Chem*. **57**, 1441 (1985).
18. E. B. Bagley. *J. Appl. Phys.* **27**, 624 (1957).
19. S. Middleman. *The Flow of High Polymers*, John Wiley, New York (1967).
20. H. M. Laun. *Rheol. Acta* **22** 171 (1983).
21. W. P. Cox and E. H. Merz. *J. Polym. Sci.* **28**, 619 (1958).
22. J. H. Elliott. *J. Appl. Polym. Sci*. **13**, 755 (1969).
23. S. Suto, J. L. White, J. F. Fellers. *Rheol. Acta* **21**, 62 (1982).
24. T. Masuda. Personal communication.
25. H. Sugiyana, D. N. Lewis, J. L. White, J. F. Fellers. *J. Appl. Polym. Sc*i. **30**, 2329 (1985).